Chapter 1

Theory

1.1 X-ray Diffraction

1.1.1 Scattering at Lattices

To elucidate the working principles behind X-ray diffraction (XRD) as a measurement method, a brief description of reciprocal space and constructive interference will be provided. Those derivations are based on Ashcroft and Mermin (1976) [1].

A periodic point-like structure with translational symmetry ("BRAVAIS lattice") can be described by three vectors $\mathbf{a}_i$ that span a so-called "unit cell". Every lattice point $\mathbf{R}$ is a linear combination of those unit cell vectors. For such a lattice, there exists a so-called "reciprocal lattice", which consists of all vectors $\mathbf{K}$ satisfying the condition[1]:

$$e^{i\langle \mathbf{K},\mathbf{R}\rangle} = 1\,. \tag{1.1}$$

This is again a BRAVAIS lattice with unit cell vectors $\mathbf{a}_j^*$:

$$\mathbf{K}_{hkl} = h\mathbf{a}_1^* + k\mathbf{a}_2^* + l\mathbf{a}_3^*\,. \tag{1.2}$$

It follows that for any i, j:

$$\langle \mathbf{a}_i^*, \mathbf{a}_j\rangle = 2\pi\delta_{ij}\,, \tag{1.3}$$

with the KRONECKER delta δ_{ij}. A major application of reciprocal space vectors is their ability to describe lattice planes. Any lattice plane can be described by the shortest possible reciprocal space vector $\mathbf{K}_{hkl}$ perpendicular to it. Consequently, the lattice plane is denoted by (hkl). The distance between equivalent lattice planes can be calculated via $d_{hkl} = |\mathbf{K}_{hkl}|^{-1}$. Note that for non-cubic crystals, the lattice plane (hkl) is in general *not* perpendicular to the lattice direction [hkl].

With those preliminarities, the conditions for constructive interference during diffraction of radiation at BRAVAIS lattices can be derived. Consider two scattering centers separated by $\mathbf{d}$. Now consider incoming radiation with wave vector $\mathbf{k}$:

$$\mathbf{k} = \frac{2\pi}{\lambda}\hat{\mathbf{n}}\,, \tag{1.4}$$

[1] The definition of $\mathbf{K}$ by (1.1) is a consequence of demanding that the plane wave described by $f_{\mathbf{K}}(\mathbf{r}) = \exp(i\langle \mathbf{K}, \mathbf{r}\rangle)$ has the same symmetry as the BRAVAIS lattice [1].

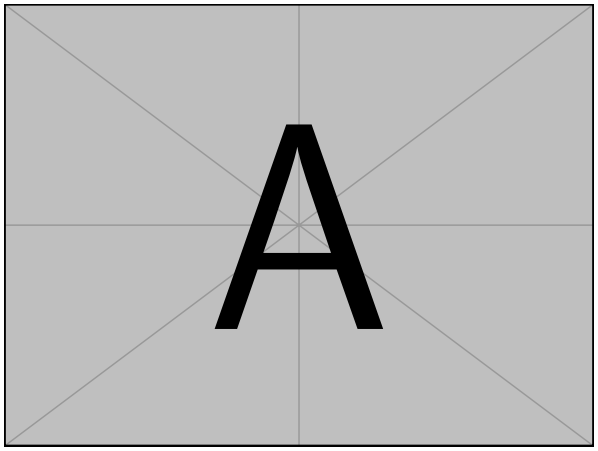

Figure 1.1: *Here comes an ashcroft-like image for the scattering geometry to derive Equ. (1.5)*

with wavelength λ and direction $\hat{\mathbf{n}}$. For the case of elastic scattering, the outcoming wave vector $\mathbf{k}'$ has the same wavelength λ but different direction $\hat{\mathbf{n}}'$. The phase difference of two photons scattered at the 1st and 2nd scattering center, respectively, can be calculated from their path difference, which reads

$$\langle \mathbf{d}, \hat{\mathbf{n}} \rangle + \langle -\mathbf{d}, \hat{\mathbf{n}}' \rangle \,. \tag{1.5}$$

Constructive interference occurs, if the phase difference is an integral multiple of the wavelength, so it must follow that

$$\langle \mathbf{d}, (\hat{\mathbf{n}} - \hat{\mathbf{n}}') \rangle = m\lambda \tag{1.6}$$

$$\Leftrightarrow \langle \mathbf{d}, (\hat{\mathbf{k}} - \hat{\mathbf{k}}') \rangle = 2\pi m \,, \tag{1.7}$$

with $m \in \mathbb{N}$. Comparing with (1.1) reveals that $\hat{\mathbf{k}} - \hat{\mathbf{k}}'$ is a reciprocal space vector, because the separation $\mathbf{d}$ of the two scattering centers is a lattice vector. So constructive interference (observing a reflex) occurs if and only if the scattering geometry (determined by angle of incidence and refraction, as well as wavelength) matches the lattice symmetry in the sense that there is a corresponding lattice translation vector $\mathbf{d}$ fulfilling Equ. (1.7). So from the "position" of reflexes, one can deduce the lattice symmetry.

Note that this description of X-ray scattering is equivalent to the Bragg condition:

$$m\lambda = 2d_{hkl} \sin(\theta) \,, \tag{1.8}$$

where the angle of incidence θ and λ are contained in $\hat{\mathbf{k}} - \hat{\mathbf{k}}'$. Furthermore, when a lattice point is not equivalent to a single atom, but represents several scattering centers, an additional geometrical structure factor has to be taken into account to determine whether a certain geometry allows reflexes. This is important, e.g., for structures with trigonal symmetry. They are described with a conventional hexagonal unit cell, although not every plane (hkl) exhibits constructive interference.

1.1.2 X-rays

Atomic distances in solids are of the order of several Å, so the radiation for probing those structures must have a similar wavelength, which turns out to be X-rays [2]. The following description of X-rays is based on Spieß (2009) [3].

The basis of any X-ray tube are high-energy electrons which are produced by thermionic emission in a cathode, which is usally made out of tungsten[2]. An electric field of several kV accelerates the electrons to the anode, where they are stopped such that around 99 % of their kinetic energy dissipates. The momentum change of electrons, which are charged particles, leads to emission of *bremsstrahlung*. Furthermore, the electrons ionize atoms of the anode material which leads to unoccupied electron states. If those states are filled by electrons with higher quantum number n, the difference in energy of those levels is emitted as radiation with a discrete spectrum, called characteristic X-ray. Important for this work is a part of the characteristic spectrum, called K-radiation, which originates in occupation of empty $1s$-orbitals. The occupying electron must come from an orbital with angular momentum quantum number $l = 1$, i.e. a p-orbital, because Δl cannot be zero. The radiation is termed Kα- or Kβ-radiation, if the previous orbital was $2p$ or $3p$, respectively. Furthermore, one distinguishes Kα_1- and Kα_2-radiation, depending on the magnetic quantum number of the previous orbital, which can be $\frac{3}{2}$ or $\frac{1}{2}$, respectively. Kα-radiation is desired for probing crystal structures.

1.2 Sesquioxides

Transparent Conductive Oxides (TCOs) are materials that combine the properties of having low absorption coefficient in the visible spectrum and being conductive at the same time [4]. The interest in these materials is motivated by possible usage in portable and flexible electronics, displays, solar cells and more [5]. Due to the restriction on only a few materials in the industry (e.g. SnO_2 and In_2O_3), investigations of new materials are required [5]. This includes fabrication of p-type TCOs as well as compounds with even larger band gaps than 3 eV, called Ultrawide-bandgap (UWBG) materials. A candidate for the latter is Ga_2O_3 with its several polymorphs [6], where the corundum structured α-Ga_2O_3 gained interest, even though its deposition has to account for parasitic growth of the thermodynamically more stable β-phase [7].

At this point, Cr_2O_3 comes in handy being a possible p-type TCO as well as being isomorphic to group-III sesquioxide α-Ga_2O_3 with quite similar lattice parameters (cf. Tab. 1.1). This enables the use of Cr_2O_3 as a buffer layer between α-Ga_2O_3 and isomorphic α-Al_2O_3 (sapphire) substrates to improve the deposition process [8]. Furthermore, Cr_2O_3 exhibits increased conductivity upon doping [9] and could thus serve as p-type component in a p-n-heterojunction with α-Ga_2O_3. In the following, an overview of the two mentioned sesquioxides will be provided with focus on the physical properties being relevant to this work.

1.2.1 Chromium Oxide

"Chromia" or "Eskolaite" is a sesquioxide composed of the transition metal chromium and oxygen with formula unit Cr_2O_3. Among other chromium oxides (e.g. metallic CrO_2, toxic CrO_3 etc.), it is the thermodynamically most stable phase [10–12], making it the abundant chromium oxide on earth [13]. Cr_2O_3 occurs mainly in the α-phase

[2]Tungsten is the element with the second highest melting point of around 3400 °C. This ensures a low contamination of the anode with cathode material.

	a	c	Ref.
α-Al_2O_3	4.76 Å	13.00 Å	Pishchik et al. (2009) [20]
α-Cr_2O_3	4.96 Å	13.59 Å	Mi et al. (2018) [13]
α-Ga_2O_3	4.98 Å	13.43 Å	Marezio and Remeika (1967) [21]

Table 1.1: Lattice constants of selected corundum structured compounds.

(described below), but a cubic spinel γ-phase with random missing Cr point defects has also been reported [10]. Henceforth, "Cr_2O_3" will refer to the α-phase.

As coating material, Cr_2O_3 is commonly used due to its high hardness and resistance against corrosion [11, 14], also explaining its use-case as component of stainless steel to form passive films [12]. Cr_2O_3 thin films absorb electromagnetic waves with wavelengths smaller than 400 nm, making it opaque in the UV-spectrum [15, 16]. It is transparent in the visible spectrum with, e.g., a reported transmittance of 40 % at 700 nm for 0.5 µm thick films by Cheng et al. (1996) [15].

Cr_2O_3 crystallizes in the corundum structure, which has trigonal symmetry (space group $R\bar{3}c$) and belongs to the hexagonal crystal family. One unit cell contains six formula units, i.e. 12 chromium cations and 18 oxygen anions [12]. The oxygen atoms arrange in a hexagonal close-packed manner, where two thirds of the formed octahedrons are filled with Cr atoms [17]. The unit cell is spanned by a principal axis, called c-axis[3], and a hexagonal basal plane with lattice constant a. The numerical values for those lattice parameters differ depending on the publication [4, 8, 13, 18, 19], and we will use the values in Tab. 1.1.

Several techniques were applied for depositing chromia thin films, including: Chemical Vapor Deposition (CVD) [22–24] on silicon and glass, Molecular Beam Epitaxy (MBE) on sapphire [4, 25], thermal evaporation on platinum [10], electron-beam evaporation on glass [11], spray pyrolysis on glass [26], radio-frequency (RF) sputtering on sapphire [8, 27, 28], reactive direct current (DC) sputtering on glass [16], reactive Pulsed Laser Deposition (PLD) on silicon [29] and sapphire [30], and non-reactive PLD on sapphire [4, 14, 31].

Electronic Structure Experimental and theoretical studies reveal that chromia exhibits a band gap of 3.2 to 3.4 eV [10, 12, 13, 19] making it a wide band gap material. This predicts insulating behavior [19], classified as both Mott-Hubbard type and charge-transfer type, which are models to describe the electronic behavior of compounds containing transition metals with partly filled $3d^n$ orbitals[4] [12, 13, 17]: Density Functional Theory (DFT) calculations show that the Cr-3d states are almost solely responsible for electronic states in the conduction band and that they are also present in the valence band [12, 13]. Thus, $3d \longrightarrow 3d$ band transitions are possible, favoring the Mott-Hubbard model of this compound [12]. Furthermore, the O-2p states are mainly present in the valence band, at similar energies as the Cr-3d states, which leads to hybridization and thus favoring the charge-transfer model [12].

[3] The spins of the Cr atoms along this direction are alternating 3 ↑ and 3 ↓ [4], making the crystal antiferromagnetic [12, 17].

[4] $n = 5$ for Cr

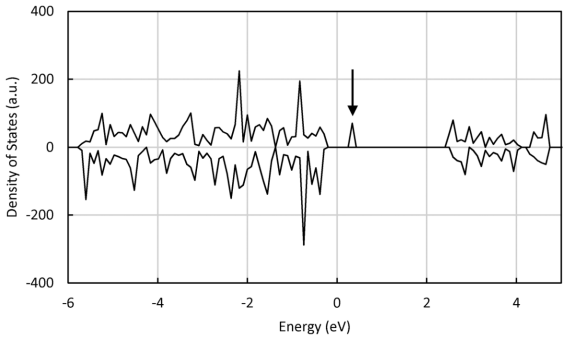

Figure 1.2: Calculated density of states (DOS) of chromia, taking a V_{Cr} into account. The arrow marks the new acceptor level. Image taken from [12].

However, several studies agree on Cr_2O_3 being a semiconductor with p-type conductivity[5] at room temperature and atmospheric conditions [12–15, 27, 29, 32]. Calculating the impact of different crystal point defects on the band structure may give insight into these observations. Indeed, when considering a missing chromium atom ("vacancy" V_{Cr}) the band structure changes in two ways: The band gap itself is reduced [13], but not in a way that it would make excitations of valence electrons into the conduction band much more probable than for defectless chromia. But additionally, there is a new band introduced slightly above the Fermi level (cf. Fig. 1.2), which acts as an unoccupied acceptor level [13]. This defect state is mainly composed of O-2p orbitals of the oxygen anions surrounding the vacancy [12]. From a more intuitive point of view, a missing neutral chromium atom effectively removes the Cr^{3+} cation as well as three electrons bound to the adjacent O^{2-} anions, thus creating three holes [12] explaining the p-type conductivity.

Note that there are also other possible defects with different effects: a chromium Frenkel point defect describes a Cr atom leaving it's position and occupying a formerly unoccupied cavity in one of the oxygen-octahedrons. This Frenkel defect actually creates a new band right below the Fermi level, acting as an occupied donor level [12]. A similar defect state is introduced by oxygen vacancies [13]. But note that the Fermi level is located only slightly above the Valence Band Maximum (VBM) and thus the new occupied donor level is not significantly closer to the Conduction Band Minimum (CBM), which means that electrons still have to overcome the band gap energy to get into conducting states. This favors the formation of holes via Cr vacancies (O-2p acceptor states) rather than electrons via Cr Frenkel defects and O vacancies (Cr-3d donor states).

Doping Several attempts have been made to alter the conductivity of chromia thin films deliberately, including incorporation of magnesium, nickel, or lithium to achieve better p-type conductivity [25]. On the other hand, incorporating titanium seems to yield electrons as majority carriers [33] due to the higher valent state of Ti when substituting Cr sites (Ti_{Cr}) [32].

[5] Cheng et al. (2001) [23] actually find Cr_2O_3 to be insulating. It is noted that they examined Cr_2O_3 as an 2 nm thick oxide surface on CrO_2 films deposited by CVD. Farrell et al. (2015) [25] also find that their high quality epitaxial films of Cr_2O_3 grown by MBE exhibit no p-type conductivity. Similar results were found by Kehoe et al. (2016) [4] for MBE and PLD deposited films.

Due to interest in the electrical properties of *p*-type TCOs, the influence on Mg-doped Cr_2O_3 thin films has been investigated by several studies [4, 9, 19, 25, 26, 31, 33]. Substituting Cr atoms with less valent hole providers – compared to structural defects of pure Cr_2O_3 – does not only allow for a more controlled defect incorporation, but is also energetically more favorable due to a lower formation energy of Mg_{Cr} compared to V_{Cr} [4]. Uekawa and Kaneko (1996) [9] report an increase in conductivity of five orders of magnitude for Cr_2O_3:Mg thin films. This result can be further improved by postannealing [25] and deposition at higher oxygen partial pressures [25, 33]. These effects are attributed to homogenization of magnesium inside the thin films and increased MgO incorporation during deposition, respectively. An observed side-effect of Mg-doping is a color change to a brownish tint [9, 19]. Uekawa and Kaneko (1996) [9] discuss that this may be the result of a mixed valence state of chromium (Cr^{4+} or Cr^{6+}), formed upon doping, as observed by X-ray Photoelectron Spectroscopy (XPS). This may establish an unoccupied state, favoring charge-transfer transitions from O-2*p* orbitals to this low-energetic state, resulting in a different visual appearance of the thin films. However, it has been shown that the overall transparency can be increased by codoping of Mg with nitrogen which also reduces the decolorization substantially [19, 26].

1.2.2 Gallium Oxide

Ga_2O_3 is a group-III sesquioxide with four different polymorphs, of which β-Ga_2O_3 is the thermodynamically most stable one at ambient conditions [6, 7, 34]. The corundum-structured α-Ga_2O_3 phase, which is of more relevance for this work, is isomorphic to Cr_2O_3 (cf. section 1.2.1), with lattice parameters as listed in Tab. 1.1. α-Ga_2O_3 is metastable [35], i.e. not favored in the first place, but remains irreversibly after formation, e.g., after phase transition from β- to α-phase at high temperatures [36]. The thermodynamic equilibrium – which determines the favored phase – can also be changed by strain due to lattice mismatch occurring during heteroepitaxy[6] [34]. This approach is of particular interest due to the possibility of deposition on cheap[7] and readily available sapphire substrates which are isomorphic to α-Ga_2O_3 [28, 35, 36]. Note that deposition of β-Ga_2O_3 on sapphire is also possible, but only with restriction to formation of more than one crystal domain [37]. On the other hand, highly crystalline [36] α-Ga_2O_3 thin films should be able to be grown without rotational domains [37].

Deposition of α-Ga_2O_3 on sapphire has been done by several deposition techniques, including [37]: Halide Vapor Phase Epitaxy (HVPE), mist CVD [38], MBE [34], Atomic Layer Deposition and metalorganic CVD. Phase-pure deposition via PLD has also been achieved [7, 34]. Despite being isomorphic to each other, α-Ga_2O_3 and sapphire still exhibit a lattice mismatch of around 4.8 % along the *a*-axis [35]. This induces semi-coherent growth with a fairly high dislocation density, which has been reported to be around $7 \times 10^{10}\,\mathrm{cm}^{-2}$ [38]. In particular, this becomes a problem regarding carrier mobility which is tremendously hindered by dislocation scattering [35].

To overcome the problems of lattice mismatch between sapphire substrates and α-Ga_2O_3 thin films, quasi-continuous gradients from Al_2O_3 to α-Ga_2O_3 have been applied,

[6] However, the possibility of formation of parasitic β-phase still has to be taken into account [7].
[7] Compared to bulk β-Ga_2O_3 substrates [35, 37].

utilizing the capability of alloying the respective compounds [39]. Furthermore, buffer layers of isomorphic Cr_2O_3 have been used to decrease the high dislocation density for deposition on *c*-oriented [8, 27] as well as *r*-oriented sapphire [28]. Deposition on other than *c*-oriented substrates also seems to decrease parasitic phases, because the suppression of crystal facets perpendicular to the principal *c*-axis may increase phase purity [40]. It has to be noted that despite the difficulties occuring upon lattice mismatch, coherent growth seems to be feasible without buffer layers for different deposition techniques, at least for some monolayers [34].

With 5.0 to 5.3 eV [37], α-Ga_2O_3 has the highest band gap of the four polymorphs [36]. Increasing or decreasing the band gap is possible by alloying with Al_2O_3 [40] or In_2O_3 [41], respectively. The crystal structure also allows for alloying with other corundum structured compounds [37], in particular other transition metal oxides such as Cr_2O_3 [27, 28]. The conduction band is mainly composed of Ga-4*s* states with an effective electron mass of $0.3\,m_e$. The valence band is very flat and mainly composed of O-2*p* orbitals, yielding a high effective electron mass and thus strong localization [36]. Next to band gap engineering, *n*-type doping via Sn or Si incorporation has been accomplished [37].

1.3 Heteroepitaxy

1.3.1 Pseudomorphic Growth

Comment: *Ist der folgende Absatz zu lang, dafür dass ich (wahrscheinlich) nur bei c-Orientierung pseudomorphic growth beobachte? Aber ich wollte gerne ausrechnen, was denn der out of plane strain* wäre, *falls es so sein sollte, damit ich später argumentieren kann, ob ich relaxed oder pseudomorphic beobachte; oder was dazwischen. Dementsprechend hab ich mich dann gezwungen gefühlt, das ganze noch mal aufzurollen. Vielleicht wäre eine Lösung, (1.10), (1.11) und (1.12) in eine Art appendix zu tun?*

When a body is deformed ("strained") from its original state of equilibrium ("bulk"), forces will arise that tend to return the body to this equilibrium. Molecular forces are the driving element behind these so-called stresses [42]. In continuum mechanics, stress σ_{ij} and strain ϵ_{kl} are symmetric rank-2 tensors that are linearly connected by the elasticity tensor with components C_{ijkl}:

$$\sigma_{ij} = C_{ijkl}\epsilon_{kl}\,, \tag{1.9}$$

which represents a set of linear equations[8].

If the in-plane (*ip*) lattice constants of two isomorphic compounds match at the interface of a heterostructure, one refers to "pseudomorphic" growth. This case confines some equations of (1.9):

1. The thin film *ip* lattice constants have to match the substrate *ip* lattice constants. This defines the magnitude of *ip* strain of the thin film material.

[8] Summation over same indices.

Table 1.2: The six independent entries of the elasticity tensor for rhombohedral Cr_2O_3 [44] and α-Ga_2O_3 [43]. All values are in units of 100 GPa.

Material	C_{11}	C_{12}	C_{13}	C_{33}	C_{44}	C_{14}
α-Cr_2O_3	3.74	1.48	1.75	3.62	1.59	−0.19
α-Ga_2O_3	3.82	1.74	1.26	3.46	0.78	−0.17

2. On the other hand, due to vertical growth, the out-of-plane (*oop*) stress of the thin film is demanded to be zero.

The resulting *oop* strain as well as non-diagonal strain components can be derived by solving the system of equations (1.9) with these two boundary conditions. In Ref. [43], formulas are derived for the unknown strains in the special case of pseudomorphic heterostructures with threefold rhombohedral symmetry. For numerical predictions of those strains, the elasticity tensor C_{ijkl} of the thin film compound has to be known. Depending on the symmetry of the crystal structure, its components collapse into a lower number of independent entries[9]: for rhombohedral crystals, six independent components are left [1]. An example of the entries of the elasticity tensor for two sesquioxides is given in Tab. 1.2.

Because of its direct influence on the *oop* lattice plane distance and thus on the XRD patterns (cf. 1.1.2), the strain component perpendicular to the sample surface, ϵ_{zz}, is of particular interest. In the following, the relevant formulas are stated as derived in Ref. [43]. They depend on the respective *ip* strains ϵ_{xx} and ϵ_{yy} caused by the lattice mismatch between film and substrate. Note that here, $\mathbf{r} = (x, y, z)$ describes coordinates in the laboratory system – in contrary to Ref. [43], where $\mathbf{r}$ and $\mathbf{r}'$ are used to describe cartesian coordinates in the crystal and laboratory system, respectively.

One derives for (11.0)-plane (*a*-orientation):

$$\epsilon_{zz,a} = -\frac{C_{13}\epsilon_{xx,a} + C_{12}\epsilon_{yy,a}}{C_{11}}\,, \tag{1.10}$$

for (10.0)-plane (*m*-orientation):

$$\epsilon_{zz,m} = -\frac{C_{13}C_{44}\epsilon_{xx,m} + (C_{12}C_{44} + C_{14}^2)\epsilon_{yy,m}}{C_{11}C_{44} - C_{14}^2}\,, \tag{1.11}$$

and for (00.1)-plane (*c*-orientation):

$$\epsilon_{zz,c} = -\frac{2C_{13}}{C_{33}}\epsilon_{yy,c}\,, \tag{1.12}$$

with $\epsilon_{xx,a} = c_S/c_F - 1$ and $\epsilon_{yy,a} = a_S/a_F - 1$, depending on the lattice parameters of substrate (a_S, c_S) and film (a_F, c_F). Note that

$$\begin{aligned}\epsilon_{xx,a} &= \epsilon_{xx,m}\,,\\ \epsilon_{yy,a} &= \epsilon_{yy,m}\,,\\ \epsilon_{yy,c} &= \epsilon_{yy,a}\,.\end{aligned}$$

[9] Due to symmetry reasons [1], the nine indices ij of the strain tensor can be unambiguously expressed by one index with six possible values: $11 \to 1$, $22 \to 2$, $33 \to 3$, $23 \to 4$, $13 \to 5$, $12 \to 6$ [43]. This allows for a 6×6-matrix representation of the elasticity tensor $C_{ijkl} \to C_{\mu\nu}$.

Table 1.3: (a) Comparison of d and d_{str}, which are the *oop* lattice plane distances for bulk Cr_2O_3 and pseudomorphic Cr_2O_3 on Al_2O_3, respectively. The corresponding *oop*-strain ϵ_{zz} is also given, as well as the corresponding angles of reflection for 2ϑ-ω-scans. (b) The resulting tilt of the thin film depending on substrate orientation for relaxed growth. The results follow from considerations on the possible slip systems and BURGER's vectors.

Orientation	(a) Pseudomorphic					(b) Relaxed	
(X-ray reflection)	d (nm)	d_{str}(nm)	ϵ_{zz}(%)	2θ (°)	$2\theta_{\mathrm{str}}$ (°)	$\theta_{T,x}$	$\theta_{T,y}$
c (00.6)	13.59	14.12	3.90	39.75	38.20	–	–
a (11.0)	2.48	2.57	3.63	36.18	34.87	no	no
m (30.0)	4.30	4.45	3.67	65.06	62.49	yes	no
r (02.4)	3.63	3.72	2.41	50.19	48.93	yes	no

For (01.2)-plane (r-orientation), the formula gets longer and can be calculated as demonstrated in Grundmann (2020) [45]. The distance of lattice planes d orthogonal to the sample surface are then strained, such that:

$$d_{\mathrm{strained}} = d(1 + \epsilon_{zz})\,. \tag{1.13}$$

Assuming pseudomorphic growth of Cr_2O_3 on Al_2O_3, one can compare the strained lattice plance distances to the unstrained bulk values, by utilizing (1.13). The numerical values, calculated from the lattice constants (Tab. 1.1) and the elasticity tensor (Tab. 1.2), are listed in Tab. 1.3a.

1.3.2 Relaxed Growth

Dislocations

When the lattice mismatch is not resolved by adaption to the substrate (cf. 1.3.1), the periodicity of the film must be disrupted via so-called dislocations to facilitate relaxed growth of the film [46]. The highest disturbance from equilibrium spacing happens close to the so-called dislocation line which draws through the material – far away from this line, the crystallinity is restored. In which fashion the distortion happens, can be characterized by the BURGER's vector **b**. The relation of the BURGER's vector to the dislocation line determines the type of the dislocation: if they are orthogonal, one refers to an *edge* dislocation; if they are parallel, one refers to a *screw* dislocation. For a so-called "perfect" dislocation[10], the BURGER's vector is a lattice translation vector. Note that in general, dislocations exhibit both edge- and screw-character [48].

Dislocations are not static, but can move ("glide") inside the crystal. The movement happens typically inside a plane which has highest density of atoms ("glide plane") and along the BURGER's vector which is responsible for the dislocation [48]. The arrangement of glide plane and direction of movement is called "slip system", e.g. for hexagonal structures, one finds $\{00.1\}/\langle 11.0\rangle$ to be one prevailing slip system [48].

[10] Also referred to as "full" dislocation [47].

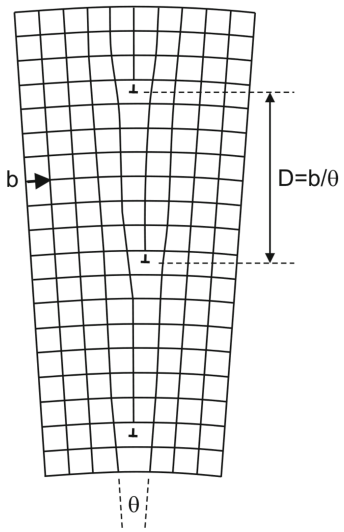

Figure 1.3: Edge dislocation with BURGER's vector perpendicular to sample surface. The normal to the surface draws horizontally in this picture. Taken from Grundmann (2016) [47] *tbd*

For heterostructures with certain slip systems, the relaxation results in an additional tilt of the deposited film. This happens because a BURGER's vector **b** has more than one component: the edge component $b_\parallel$ causes strain relaxation along $b_\parallel$; but if **b** also exhibits a component $b_\perp$ orthogonal to the sample surface and the dislocation line, a tilt angle θ_T will result between substrate and relaxed film:

$$\theta_{T,i} = \epsilon_{ii} \frac{b_{i,\perp}}{b_{i,\parallel}} , \tag{1.14}$$

where i denotes the axis of strain relaxation. This is schematically depicted in Fig. 1.3.

Slip Systems for Sesquioxide Heterostructures

For heteroepitaxial $(Al_xGa_{1-x})_2O_3$-Al_2O_3 systems with low Al content, studies have been conducted on the prevailing relaxation mechanisms for r-oriented [49, 50], as well as a- and m-oriented [46] growth directions. In the following, those results will be summarized. Note that the x-axis points along the c-axis for m- and a-oriented heterostructures, and similarly along the projection of the c-axis on the sample surface for r-oriented heterostructures.

(01.2)-plane (r-orientation) The two relevant slip systems are $\{00.1\}/\frac{1}{3}\langle 11.0\rangle$ and $\{11.0\}/\frac{1}{3}\langle 1\bar{1}.1\rangle$, which contain the "basal" and "prismatic" glide plane, respectively [49]. The former allows relaxation along the direction containing the projection of the c-axis (x-axis), whereas the latter allows relaxation perpendicular to it (y-axis). For the basal system, one can determine two possible independent BURGER's vectors $\mathbf{b}_c$ with differing screw components but otherwise same tilt and edge components $b_{c,\perp}$ and $b_{c,\parallel}$, respectively. The tilt along x-direction can then be calculated via:

$$\theta_{T,x} = \epsilon_{xx} \frac{b_{c,\perp}}{b_{c,\parallel}} = \frac{1}{\sqrt{3}} \zeta_F \epsilon_{xx} . \tag{1.15}$$

with $\zeta_F = c_F/a_F$. For the prismatic slip system, the possible BURGER's vectors facilitate relaxation along the y-direction via $b_{a,\parallel}$. But in contrast to the basal system, the tilt components $b_{a,\perp}$ cancel out on average, thus resulting in no net tilt along the y-direction: $\theta_{T,y} = 0$.

(10.0)-plane (*m*-orientation) Neither basal (00.1) nor prismatic (11.0) and (10.0) slip systems can resolve strain along the x-axis: The (00.1)-plane is perpendicular to the surface and x-direction, thus the BURGER's vector can only have components in the y-z-plane. But for strain release along x, the BURGER's vector should have some component in this direction, which cannot be the case. The prismatic planes, on the other hand, are perpendicular to the surface but parallel to the x-axis. This results in a dislocation line along the x-direction. To release strain, the BURGER's vector would have x-component, which does not apply for edge dislocations. So the prevailing slip system must have (01.2)-plane (r-orientation) or (11.2)-plane (s-orientation) character, which are called "pyramidal" slip systems. Three different r-planes contribute to strain release, because there is dislocation line component along the y-axis and BURGER's vector's components along the x-axis. With (1.14) and plugging in the possible BURGER's vectors one finds:

$$\theta_{T,x} = \frac{2}{3} \frac{\sqrt{3}}{\frac{20\zeta}{24+6\zeta^2} + \zeta} \left(\frac{c_S}{c_F} - 1 \right) \tag{1.16}$$

(11.0)-plane (*a*-orientation) The same argument as for the m-oriented heterestructure holds, why only pyramidal slip systems are possible. But in this case, only two r-planes contribute to strain relaxation, because the third plane is perpendicular to the surface, thus can only exhibit BURGER's vectors without in-plane components which results in no possible edge dislocations. Furthermore, in this case, the BURGER's vectors of the two remaining r-planes have opposite tilt components, i.e. they point outwards and inwards of the surface, respectively. Regarding (1.14), this will result in no net tilt of the thin film.

Bibliography

[1] Neil W. Ashcroft and N. David Mermin. *Solid State Physics*. Saunders College Publishing, 1976. 826 pp.

[2] George F. Harrington and José Santiso. "Back-to-Basics tutorial: X-ray diffraction of thin films". In: *Journal of Electroceramics* 47.4 (2021), pp. 141–163. ISSN: 1385-3449, 1573-8663. DOI: 10.1007/s10832-021-00263-6.

[3] Lothar Spieß, ed. *Moderne Röntgenbeugung: Röntgendiffraktometrie für Materialwissenschaftler, Physiker und Chemiker*. 2., überarb. und erw. Aufl. Studium. Wiesbaden: Vieweg + Teubner, 2009. 564 pp. ISBN: 978-3-8351-0166-1.

[4] Aoife B Kehoe et al. "Assessing the potential of Mg-doped Cr_2O_3 as a novel p-type transparent conducting oxide". In: *Journal of Physics: Condensed Matter* 28.12 (2016), p. 125501. ISSN: 0953-8984, 1361-648X. DOI: 10.1088/0953-8984/28/12/125501.

[5] David S. Ginley, ed. *Handbook of Transparent Conductors*. Boston, MA: Springer US, 2011. ISBN: 978-1-4419-1637-2 978-1-4419-1638-9. DOI: 10.1007/978-1-4419-1638-9.

[6] Anna Hassa, Marius Grundmann, and Holger Von Wenckstern. "Progression of group-III sesquioxides: epitaxy, solubility and desorption". In: *Journal of Physics D: Applied Physics* 54.22 (2021), p. 223001. ISSN: 0022-3727, 1361-6463. DOI: 10.1088/1361-6463/abd4a4.

[7] Clemens Petersen et al. "PLD of α-Ga_2O_3 on m-plane Al_2O_3: Growth regime, growth process, and structural properties". In: *APL Materials* 11.6 (2023), p. 061122. ISSN: 2166-532X. DOI: 10.1063/5.0149797.

[8] S.I. Stepanov et al. "HVPE growth of corundum-structured α-Ga2O3 on sapphire substrates with α-Cr2O3 buffer layer". In: *Materials Physics and Mechanics* 47 (2021), pp. 577–581. DOI: 10.18149/MPM.4742021_4.

[9] N. Uekawa and K. Kaneko. "Dopant Reduction in p-Type Oxide Films upon Oxygen Absorption". In: *The Journal of Physical Chemistry* 100.10 (1996), pp. 4193–4198. ISSN: 0022-3654, 1541-5740. DOI: 10.1021/jp952784m.

[10] P. S. Robbert et al. "Novel electronic and magnetic properties of ultrathin chromium oxide films grown on Pt(111)". In: *Journal of Vacuum Science & Technology A: Vacuum, Surfaces, and Films* 16.3 (1998), pp. 990–995. ISSN: 0734-2101, 1520-8559. DOI: 10.1116/1.581283.

[11] M.F. Al-Kuhaili and S.M.A. Durrani. "Optical properties of chromium oxide thin films deposited by electron-beam evaporation". In: *Optical Materials* 29.6 (2007), pp. 709–713. ISSN: 09253467. DOI: 10.1016/j.optmat.2005.11.020.

[12] François Lebreau et al. “Structural, Magnetic, Electronic, Defect, and Diffusion Properties of Cr_2O_3: A DFT+U Study”. In: *The Journal of Physical Chemistry C* 118.31 (2014), pp. 18133–18145. ISSN: 1932-7447. DOI: 10.1021/jp5039943.

[13] Zhishan Mi et al. “The effects of strain and vacancy defects on the electronic structure of Cr_2O_3”. In: *Computational Materials Science* 144 (2018), pp. 64–69. ISSN: 09270256. DOI: 10.1016/j.commatsci.2017.12.012.

[14] Jarnail Singh et al. “Structural, optical and electrical characterization of epitaxial Cr_2O_3 thin film deposited by PLD”. In: *Materials Research Express* 6.10 (2019), p. 106406. ISSN: 2053-1591. DOI: 10.1088/2053-1591/ab3543.

[15] Chun-Shen Cheng, H. Gomi, and H. Sakata. “Electrical and Optical Properties of Cr_2O_3 Films Prepared by Chemical Vapour Deposition”. In: *Physica Status Solidi (a)* 155.2 (1996), pp. 417–425. ISSN: 00318965, 1521396X. DOI: 10.1002/pssa.2211550215.

[16] Cecilia Guillén and José Herrero. “Structural Changes Induced by Heating in Sputtered NiO and Cr_2O_3 Thin Films as p-Type Transparent Conductive Electrodes”. In: *Electronic Materials* 2.2 (2021), pp. 49–59. ISSN: 2673-3978. DOI: 10.3390/electronicmat2020005.

[17] M. Catti et al. “Electronic, magnetic and crystal structure of Cr_2O_3 by theoretical methods”. In: *Journal of Physics and Chemistry of Solids* 57.11 (1996), pp. 1735–1741. ISSN: 00223697. DOI: 10.1016/0022-3697(96)00034-0.

[18] Larry W. Finger and Robert M. Hazen. “Crystal structure and isothermal compression of Fe_2O_3, Cr_2O_3, and V_2O_3 to 50 kbars”. In: *Journal of Applied Physics* 51.10 (1980), pp. 5362–5367. ISSN: 0021-8979, 1089-7550. DOI: 10.1063/1.327451.

[19] Elisabetta Arca et al. “Effect of Chemical Precursors On the Optical and Electrical Properties of p-Type Transparent Conducting Cr_2O_3:(Mg,N)”. In: *The Journal of Physical Chemistry C* 117.42 (2013), pp. 21901–21907. ISSN: 1932-7447. DOI: 10.1021/jp404230k.

[20] Valerian Pishchik, Leonid A. Lytvynov, and Elena R. Dobrovinskaya. *Sapphire: Material, Manufacturing, Applications*. Boston, MA: Springer US, 2009. ISBN: 978-0-387-85694-0 978-0-387-85695-7. DOI: 10.1007/978-0-387-85695-7.

[21] M. Marezio and J. P. Remeika. “Bond lengths in the α-Ga_2O_3 structure and the high-pressure phase of $Ga_{2-x}Fe_xO_3$”. In: *The Journal of Chemical Physics* 46.5 (1967), pp. 1862–1865. ISSN: 0021-9606, 1089-7690. DOI: 10.1063/1.1840945.

[22] Ruihua Cheng, C.N. Borca, and P.A. Dowben. “Selective Area Chemical Vapor Deposition of Chromium Oxides”. In: *MRS Proceedings* 614 (2000), F10.4.1. ISSN: 0272-9172, 1946-4274. DOI: 10.1557/PROC-614-F10.4.1.

[23] Ruihua Cheng et al. “Characterization of the native Cr_2O_3 oxide surface of CrO_2”. In: *Applied Physics Letters* 79.19 (2001), pp. 3122–3124. ISSN: 0003-6951, 1077-3118. DOI: 10.1063/1.1416474.

[24] Ruihua Cheng et al. "Potential phase control of chromium oxide thin films prepared by laser-initiated organometallic chemical vapor deposition". In: *Applied Physics Letters* 78.4 (2001), pp. 521–523. ISSN: 0003-6951, 1077-3118. DOI: 10.1063/1.1343846.

[25] L. Farrell et al. "Conducting mechanism in the epitaxial p-type transparent conducting oxide Cr_2O_3:Mg". In: *Physical Review B* 91.12 (2015), p. 125202. ISSN: 1098-0121, 1550-235X. DOI: 10.1103/PhysRevB.91.125202.

[26] E. Arca, K. Fleischer, and I. V. Shvets. "Magnesium, nitrogen codoped Cr_2O_3: A p-type transparent conducting oxide". In: *Applied Physics Letters* 99.11 (2011), p. 111910. ISSN: 0003-6951. DOI: 10.1063/1.3638461.

[27] Alexander Polyakov et al. "Electrical properties of α-Ga2O3 films grown by halide vapor phase epitaxy on sapphire with α-Cr2O3 buffers". In: *Journal of Applied Physics* 131.21 (2022), p. 215701. ISSN: 0021-8979, 1089-7550. DOI: 10.1063/5.0090832.

[28] Alexander Polyakov et al. "Effects of sapphire substrate orientation on Sn-doped α-Ga_2O_3 grown by halide vapor phase epitaxy using α-Cr_2O_3 buffers". In: *Journal of Physics D: Applied Physics* 55.49 (2022), p. 495102. ISSN: 0022-3727, 1361-6463. DOI: 10.1088/1361-6463/ac962f.

[29] Anna Caricato et al. "Deposition of chromium oxide thin films with large thermoelectromotive force coefficient by reactive pulsed laser ablation". In: *Journal of Optoelectronics and Advanced Materials* 12 (2010), p. 427.

[30] Sandhyarani Punugupati, Jagdish Narayan, and Frank Hunte. "Room temperature ferromagnetism in epitaxial Cr_2O_3 thin films grown on r-sapphire". In: *Journal of Applied Physics* 117.19 (2015), p. 193907. ISSN: 0021-8979, 1089-7550. DOI: 10.1063/1.4921435.

[31] Elisabetta Arca et al. "Valence band modification of Cr_2O_3 by Ni-doping: creating a high figure of merit p-type TCO". In: *Journal of Materials Chemistry C* 5.47 (2017), pp. 12610–12618. ISSN: 2050-7534. DOI: 10.1039/C7TC03545D.

[32] P. Kofstad and K. P. Lillerud. "On High Temperature Oxidation of Chromium: II . Properties of and the Oxidation Mechanism of Chromium". In: *Journal of The Electrochemical Society* 127.11 (1980), pp. 2410–2419. ISSN: 0013-4651, 1945-7111. DOI: 10.1149/1.2129481.

[33] A Holt and P Kofstad. "Electrical conductivity and defect structure of Cr_2O_3. II. Reduced temperatures (<∼1000 °C)". In: *Solid State Ionics* 69.2 (1994), pp. 137–143. ISSN: 01672738. DOI: 10.1016/0167-2738(94)90402-2.

[34] Robert Schewski et al. "Epitaxial stabilization of pseudomorphic α-Ga_2O_3 on sapphire (0001)". In: *Applied Physics Express* 8.1 (2015), p. 011101. ISSN: 1882-0778, 1882-0786. DOI: 10.7567/APEX.8.011101.

[35] Kentaro Kaneko et al. "Progress in α-Ga_2O_3 for practical device applications". In: *Japanese Journal of Applied Physics* 62 (SF 2023), SF0803. ISSN: 0021-4922, 1347-4065. DOI: 10.35848/1347-4065/acd125.

[36] S. J. Pearton et al. "A review of Ga_2O_3 materials, processing, and devices". In: *Applied Physics Reviews* 5.1 (2018), p. 011301. ISSN: 1931-9401. DOI: 10.1063/1.5006941.

[37] Duyoung Yang et al. "Epitaxial growth of alpha gallium oxide thin films on sapphire substrates for electronic and optoelectronic devices: progress and perspective". In: *Electronic Materials Letters* 18.2 (2022), pp. 113–128. ISSN: 1738-8090, 2093-6788. DOI: 10.1007/s13391-021-00333-5.

[38] Kentaro Kaneko et al. "Evaluation of misfit relaxation in α-Ga_2O_3 epitaxial growth on α-Al_2O_3 substrate". In: *Japanese Journal of Applied Physics* 51 (2R 2012), p. 020201. ISSN: 0021-4922, 1347-4065. DOI: 10.1143/JJAP.51.020201.

[39] Riena Jinno et al. "Reduction in edge dislocation density in corundum-structured α-Ga_2O_3 layers on sapphire substrates with quasi-graded α-$(Al,Ga)_2O_3$ buffer layers". In: *Applied Physics Express* 9.7 (2016), p. 071101. ISSN: 1882-0778, 1882-0786. DOI: 10.7567/APEX.9.071101.

[40] Riena Jinno et al. "Crystal orientation dictated epitaxy of ultrawide-bandgap 5.4- to 8.6-eV α-$(AlGa)_2O_3$ on m-plane sapphire". In: *Science Advances* 7.2 (2021), eabd5891. ISSN: 2375-2548. DOI: 10.1126/sciadv.abd5891.

[41] Anna Hassa et al. "Control of phase formation of $(Al_xGa_{1-x})_2O_3$ thin films on c-plane Al_2O_3". In: *Journal of Physics D: Applied Physics* 53.48 (2020), p. 485105. ISSN: 0022-3727, 1361-6463. DOI: 10.1088/1361-6463/abaf7d.

[42] L. D. Landau and E. M. Lifshitz. *Theory of Elasticity*. Course of Theoretical Physics vol. 7. Pergamon Press Ltd., 1970. 165 pp. ISBN: 978-0-08-057069-3.

[43] Marius Grundmann. "Elastic theory of pseudomorphic monoclinic and rhombohedral heterostructures". In: *Journal of Applied Physics* 124.18 (2018), p. 185302. ISSN: 0021-8979, 1089-7550. DOI: 10.1063/1.5045845.

[44] H.L. Alberts and J.C.A. Boeyens. "The elastic constants and distance dependence of the magnetic interactions of Cr_2O_3". In: *Journal of Magnetism and Magnetic Materials* 2.4 (1976), pp. 327–333. ISSN: 03048853. DOI: 10.1016/0304-8853(76)90044-5.

[45] Marius Grundmann. "A most general and facile recipe for the calculation of heteroepitaxial strain". In: *physica status solidi (b)* 257.12 (2020), p. 2000323. ISSN: 0370-1972, 1521-3951. DOI: 10.1002/pssb.202000323.

[46] Max Kneiß et al. "Strain states and relaxation for α-$(Al_xGa_{1-x})_2O_3$ thin films on prismatic planes of α-Al_2O_3 in the full composition range: Fundamental difference of a- and m-epitaxial planes in the manifestation of shear strain and lattice tilt". In: *Journal of Materials Research* 36.23 (2021), pp. 4816–4831. ISSN: 0884-2914, 2044-5326. DOI: 10.1557/s43578-021-00375-3.

[47] Marius Grundmann. *The Physics of Semiconductors: An Introduction Including Nanophysics and Applications*. Graduate Texts in Physics. Cham: Springer International Publishing, 2016. ISBN: 978-3-319-23879-1 978-3-319-23880-7. URL: http://link.springer.com/10.1007/978-3-319-23880-7.

[48] Derek Hull and D. J. Bacon. *Introduction to Dislocations*. 5th ed. Elsevier Ltd., 2011. 268 pp. ISBN: 978-0-08-096673-1.

[49] M. Grundmann and M. Lorenz. "Anisotropic strain relaxation through prismatic and basal slip in α-(Al, Ga)$_2$O$_3$ on R-plane Al$_2$O$_3$". In: *APL Materials* 8.2 (2020), p. 021108. ISSN: 2166-532X. DOI: 10.1063/1.5144744.

[50] M. Grundmann, T. Stralka, and M. Lorenz. "Epitaxial growth and strain relaxation of corundum-phase (Al,Ga)$_2$O$_3$ thin films from pulsed laser deposition at 1000 °C on r-plane Al$_2$O$_3$". In: *Applied Physics Letters* 117.24 (2020), p. 242102. ISSN: 0003-6951, 1077-3118. DOI: 10.1063/5.0030675.